

## Chapter 2

# MR Motion Correction of 3D Affine Deformations

This chapter presents an MR motion correction technique for objects undergoing a 3D affine transformation [65, 66]. This class of deformations includes all global linear space warping functions, and is formalized in Section 2.1.1. Affine motion correction could be used to compensate for the respiratory motion and deformation of the heart, coronary arteries, liver and kidneys. It is thought that the changes in these organs due to respiration are more complicated than rigid transformations, but may be well modeled by relatively simple deformations. An analysis of the affine motion of the right coronary artery was recently presented in [67].

Building on the affine theorem for the 2D Fourier transform [68], the dimension three analog is derived, and the relationship between the  $k$ -space of an imaged volume, and the  $k$ -space of a 3D affine transformation of the volume is developed in Section 2.1.2. A simulation validating the proposed motion correction technique is presented in Section 2.2.2. Finally, a discussion of practical considerations for implementing 3D affine motion correction during an MR image acquisition is presented in Section 2.3.

---

Work from this chapter was presented at the International Society for Magnetic Resonance in Medicine 2003 Scientific Meeting [65].

## 2.1 Theory

### 2.1.1 3D Affine Transformation

The class of 3D affine transformations  $\{\mathcal{A} : \mathbb{R}^3 \rightarrow \mathbb{R}^3\}$  describes a global space warping with twelve degrees of freedom. The 3D affine transformation of a point  $\mathbf{x} = (x, y, z)^T$  can be written as

$$\mathcal{A}(\mathbf{x}) = \mathbf{A} \cdot \mathbf{x} + \mathbf{t} \quad (2.1)$$

where

$$\mathbf{A} = \begin{bmatrix} a_{1,1} & a_{1,2} & a_{1,3} \\ a_{2,1} & a_{2,2} & a_{2,3} \\ a_{3,1} & a_{3,2} & a_{3,3} \end{bmatrix} \text{ and } \mathbf{t} = \begin{bmatrix} t_x \\ t_y \\ t_z \end{bmatrix}. \quad (2.2)$$

The nine independent parameters  $a_{i,j}$  of  $\mathbf{A}$  represent a 3D linear transformation, and the matrix  $\mathbf{T}$  represents a 3D translation.

The matrix  $\mathbf{A}$  can be decomposed into components representing a 3D rotation, scaling (dilation or compression), and shear. For the remainder of this paper, we will use the decomposition in which

$$\mathbf{A} = \mathbf{R}(\phi, \theta, \psi) \begin{bmatrix} 1 & S_{xy} & S_{xz} \\ 0 & 1 & S_{yz} \\ 0 & 0 & 1 \end{bmatrix} \begin{bmatrix} S_x & 0 & 0 \\ 0 & S_y & 0 \\ 0 & 0 & S_z \end{bmatrix} \quad (2.3)$$

where  $\mathbf{R}(\phi, \theta, \psi)$  is any 3x3 rotation matrix,  $\{S_{xy}, S_{xz}, S_{yz}\}$  are 3D shear parameters, and  $\{S_x, S_y, S_z\}$  are scale factors in three orthogonal directions. The use of an upper triangular shear matrix is arbitrary, but the choice simplifies the analysis of shear presented in the Discussion section by preserving the object's profile in the slice selection direction. Other modes of shear deformation can be decomposed into an upper triangular shear matrix and some rotational and scaling components.

### 2.1.2 Space–Frequency Duality of 3D Affine Transformations

Magnetic resonance imaging techniques acquire data in  $k$ -space, the Fourier space representation of the imaging volume. Therefore, it is important to understand how the spatial 3D affine transformation of an object affects its  $k$ -space representation. Suppose an imaging volume  $V \in \mathbb{C}^3$  has an equivalent Fourier representation  $F \in \mathbb{C}^3$ . Now, consider that  $V' \in \mathbb{C}^3$  is the 3D affine transformation of  $V$ ,

$$V \xrightarrow{\mathcal{A}} V' \quad (2.4)$$

and  $F' \in \mathbb{C}^3$  is the Fourier equivalent of  $V'$ . How are  $F$  and  $F'$  related?

Using properties of the Fourier transform, it is shown in the Appendix that the spatial frequency  $\mathbf{k} = (k_x, k_y, k_z) \in F$  becomes  $\mathbf{k}' = (k'_x, k'_y, k'_z) \in F'$ , according to

$$\mathbf{k}' = \mathbf{A}^{-T} \mathbf{k} , \quad (2.5)$$

where  $\mathbf{A}^{-T}$  is the transpose of the inverse of the 3x3 matrix component of the spatial 3D affine transformation  $\mathcal{A}$  defined in Equation (2.1). Thus, the relationship between  $F$  and  $F'$  can be written as:

$$F(\mathbf{k}) = \frac{e^{i2\pi(\mathbf{k}' \cdot \mathbf{t})}}{|\det(\mathbf{A})|} F'(\mathbf{k}') \quad (2.6)$$

where  $\mathbf{t}$  is the 3D translation component of  $\mathcal{A}$ , and  $\det(\mathbf{A})$  is the determinant of  $\mathbf{A}$ . Using the decomposition of  $\mathbf{A}$  from equation (2.3), where the rotation and shear matrices are known to be orthogonal with a determinant of one, equation (2.6) can be written as

$$F(\mathbf{k}) = \frac{e^{i2\pi(\mathbf{k}' \cdot \mathbf{t})}}{|S_x S_y S_z|} F'(\mathbf{k}') \quad (2.7)$$

It can be appreciated from equations (2.5) and (2.7) that in response to a spatial 3D affine transformation, the Fourier representation undergoes a related (transposed inverse) 3D affine transformation, with a zero translation component (Figure 2.1). In addition, the Fourier space may experience phase differences due to spatial translation, and magnitude scaling due to dilation or compression.

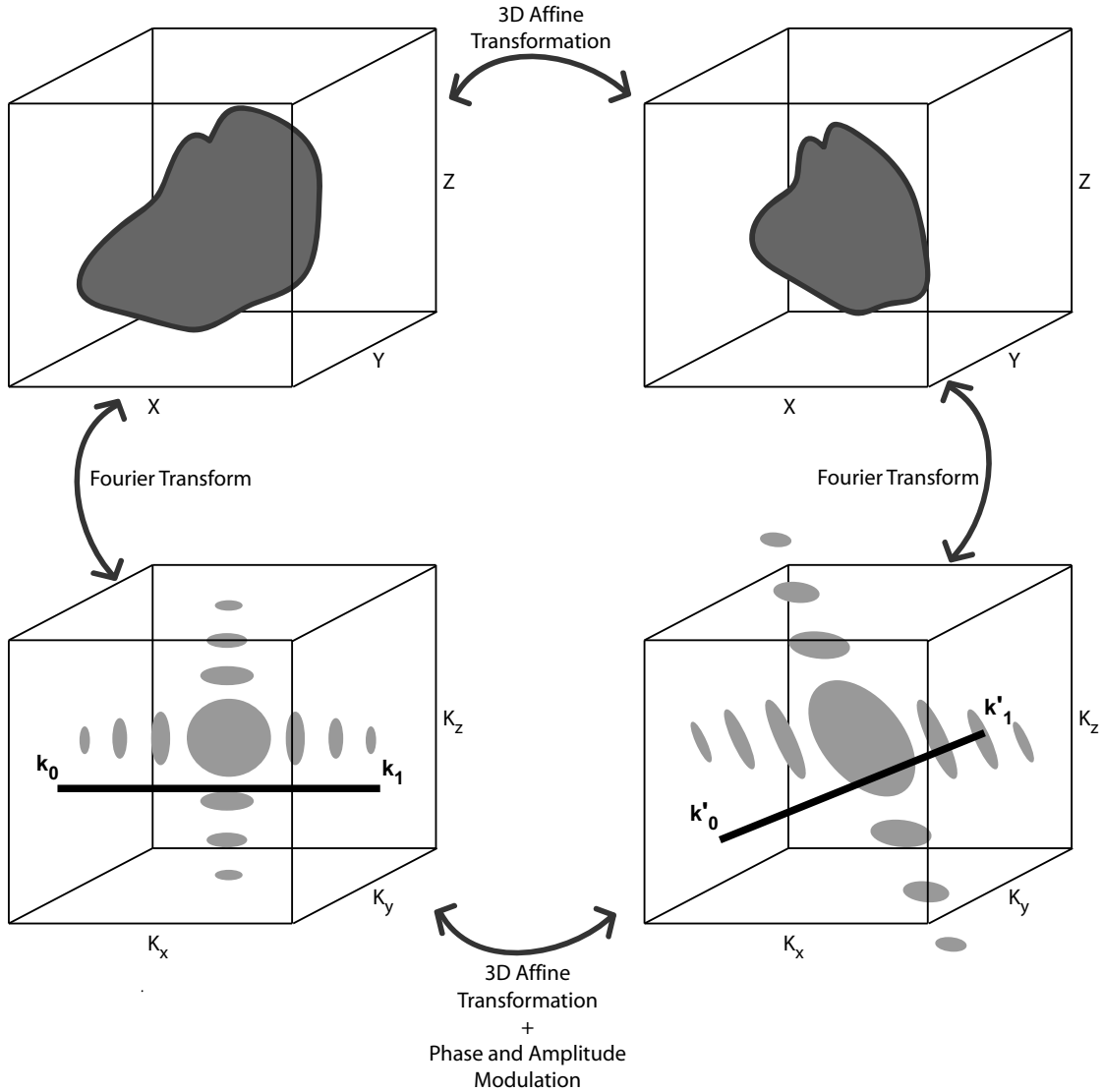


Figure 2.1: The space–frequency duality of 3D affine transformations. A spatial 3D affine deformation of an object, is equivalent to a 3D affine deformation, with a phase and amplitude modulation of the object’s frequency representation ( $k$ -space). The space and frequency affine transformations are related by Eqs. (2.5) and (2.7).

## 2.2 Computer Simulation: Prospective Correction

### 2.2.1 Method

A computer simulation was performed to validate the proposed 3D affine motion correction method. The implicit algebraic equation  $(x^2 + 2y^2 + z^2 - 1)^3 - z^3(x^2 + 0.1y^2) < 0$  was used to construct a binary 3D heart phantom in a volume of 64x64x64 voxels (Figure 2.2). The phantom was deformed by a 3D affine transformation whose magnitude varied sinusoidally, and was characterized by the twelve parameters  $\{\bar{\theta}, \bar{\psi}, \bar{\phi}, \bar{T}_x, \bar{T}_y, \bar{T}_z, \bar{S}_x, \bar{S}_y, \bar{S}_z, \bar{S}_{xy}, \bar{S}_{xz}, \bar{S}_{yz}\}$  as described in Section 2.1.1. A sinusoidal function was used because of its simplicity, and its similarity to the respiratory motion driving function.

The motion was periodic with frequency  $f$ , so that at time  $t$ , the transformation parameters were calculated using

$$p = \bar{p} \sin(2\pi ft) \quad (2.8)$$

where  $\bar{p}$  represents any of the shear, rotation, or translation parameters. For dilation or compression, we used

$$q = 1 + \bar{q} \sin(2\pi ft) \quad (2.9)$$

where  $\bar{q}$  represents any of the scaling parameters.

A 3D Fourier imaging technique (spin-warp) was implemented. MR signals were generated by calculating the Fourier coefficients of the  $64^3$  volume for given spatial frequencies. Phantom motion was simulated by cycling through different volumes, each with a representation of the heart phantom at a different state of its deformation. The time interval between two successive  $k$ -space line acquisitions (TR), was  $0.05/f$ , which required 20 volumetric data sets of the deforming phantom. For example, if the phantom was representative of a physiological motion with a frequency of 1 Hz, the simulated TR would be 50 ms.

The  $k$ -space volume was filled using a standard top-to-bottom strategy on a rectilinear 3D grid, with the readout direction along the spatial Y axis. It was assumed that there was no motion during the echo readout, and that imaging conditions were

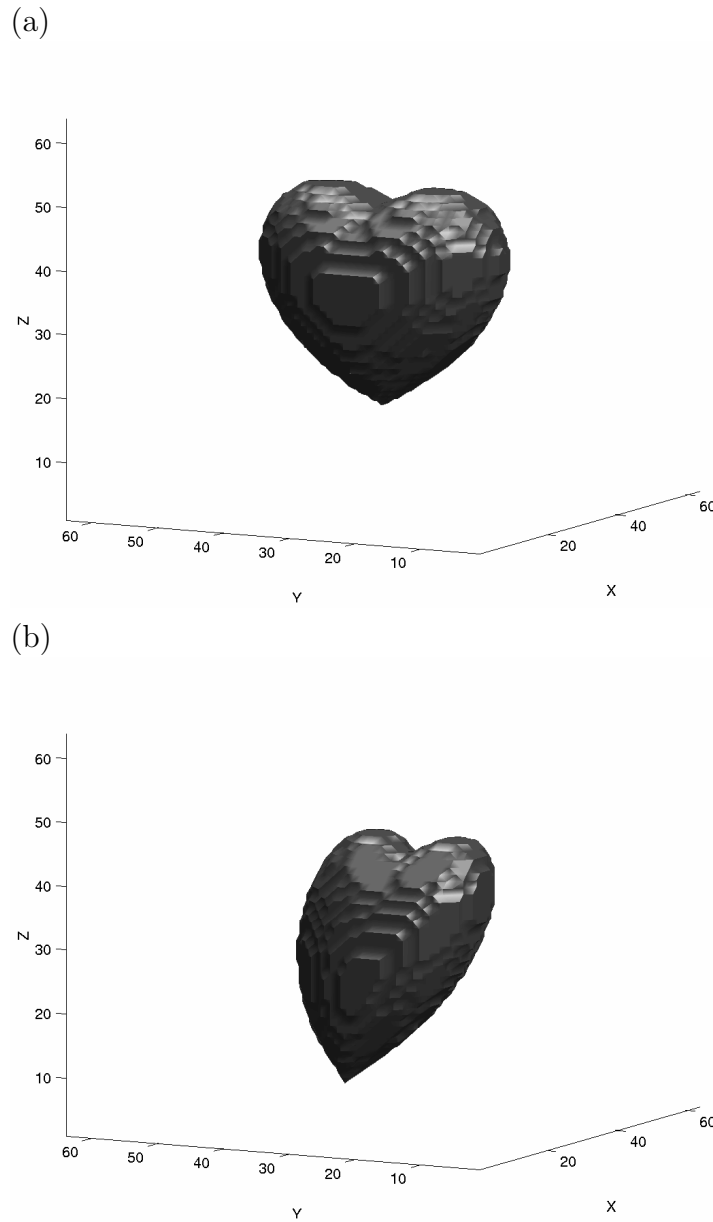


Figure 2.2: (a) The discrete 3D heart phantom constructed using the implicit algebraic equation  $(x^2 + 2y^2 + z^2 - 1)^3 - z^3(x^2 + 0.1y^2) < 0$ . (b) A 3D affine deformation of the phantom.

ideal, where the signal is obtained as a mathematical Fourier transform, so that  $T_1$  and  $T_2$  decay, flip angle, and time to echo are unimportant.

Affine motion correction was implemented as a prospective strategy (Figure 2.3). When acquiring a given  $k$ -space line, the phase of the periodic deformation was known, and therefore, the affine deformation parameters were also known *a priori*. Using equations (2.5) and (2.7), a new Fourier space trajectory for the deformed dataset volume was calculated. Data was acquired along this modified path, and placed into the reference undeformed  $k$ -space volume along the original rectilinear trajectory. Re-gridding is not needed since the data is stored in the 3D matrix along the prescribed regular trajectories. The resulting volume of  $k$ -space, was Fourier transformed to obtain a 3D image dataset.

## 2.2.2 Results

Results of the computer simulation validating the proposed 3D affine motion correction method are presented in Figure 2.4. The parameters used for the simulation were:  $\bar{\theta} = -0.35$  radians,  $\bar{T}_x = \bar{T}_y = 2$  voxels,  $\bar{T}_z = -8$  voxels,  $\bar{S}_x = -0.2$ ,  $\bar{S}_z = 0.3$ ,  $\bar{S}_{xy} = 0.5$ , and  $\bar{\psi} = \bar{\phi} = \bar{S}_y = \bar{S}_{xz} = \bar{S}_{yz} = 0$ . Recall, that using Equation (2.9),  $\bar{S}_y = 0$  corresponds to unity scaling ( $S_y = 1$ ).

Columns I and II show three orthogonal slices through the undeformed and maximally deformed binary heart phantom. Images in column III demonstrate the severe artifacts that arise during an uncorrected acquisition as a result of the 3D affine deformation.

The images in column IV demonstrate the artifacts that are due to 3D shear. The simulation for this column included correction for 3D translation, rotation, and scaling – deformation modes for which correction has been previously discussed in the literature [47, 57, 54].

The images of column V demonstrate the success of the proposed correction method for 3D affine deformation of the imaging volume. The small artifacts still present in the images of column V are caused by the discrete nature of the phantom. The heart phantom was modeled analytically, the prescribed transformations

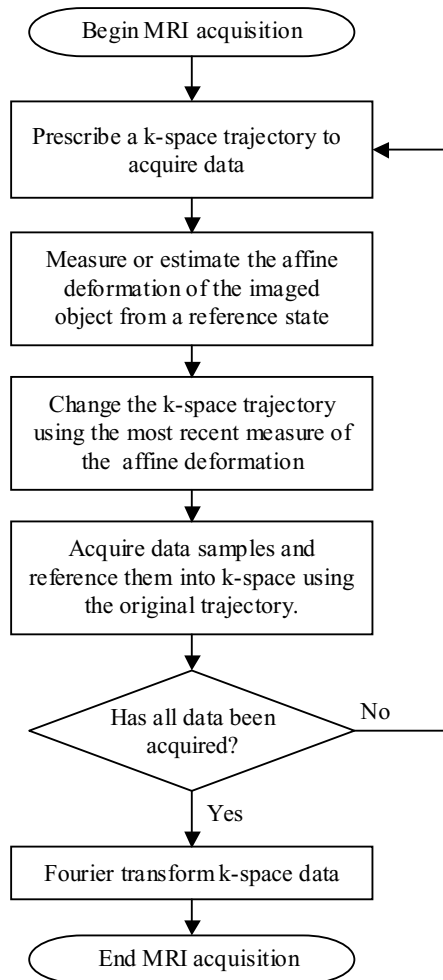


Figure 2.3: Flow diagram for prospective 3D affine motion correction.

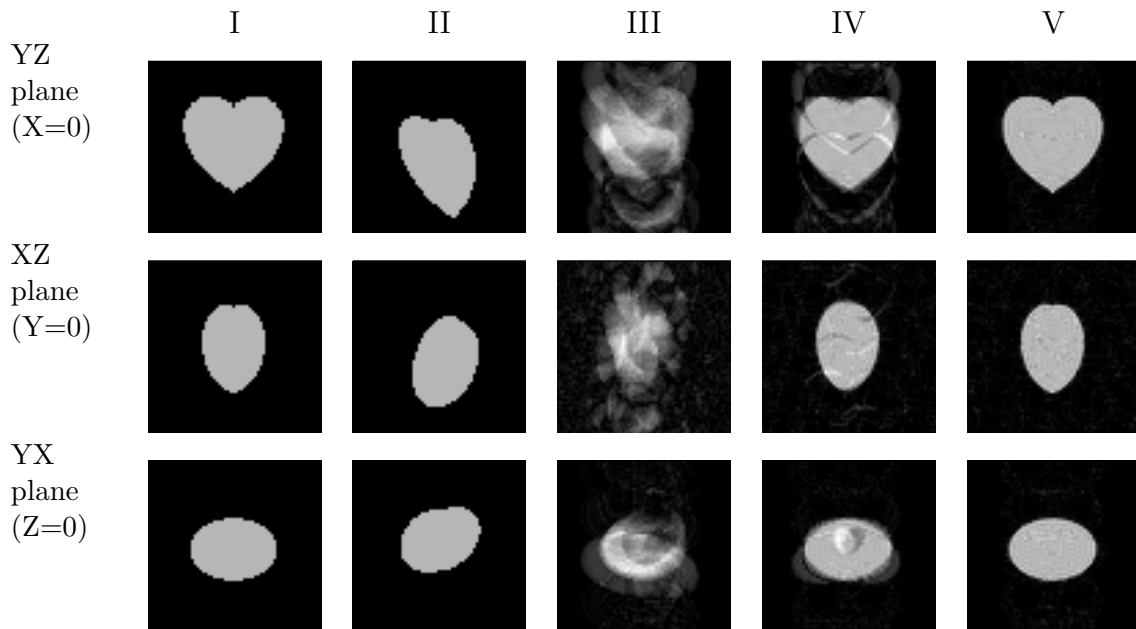


Figure 2.4: Three orthogonal slices through the imaging volume. Columns I and II show the binary phantom in the undeformed (see Figure 2.2) and maximally deformed states, respectively. A simulated 3D spin-warp acquisition of the periodically deforming phantom results in significant ghosting artifacts (III). Correction for the known 3D translation, rotation, and scaling components of the 3D affine deformation improves the quality of the images (column IV), but artifacts due to uncompensated shearing remains. In column V, images obtained with 3D affine motion correction for a known deformation.

were applied to the phantom in the continuous domain, and then the model was discretized onto a  $64^3$  volume for computational purposes. So, even though the affine transformation is known, the relationship between the discrete model volumes is not perfect.

## 2.3 Discussion

Artifacts caused by motion during MR imaging have been well studied, and over the years, many techniques have been proposed to correct for them. These efforts have almost exclusively focused on the correction of translation, rotation, and scaling of the imaged object. As the imaging hardware and methods improve, both in speed and sensitivity, new applications for MR imaging are emerging. With higher spatial and temporal resolution requirements, comes the need for higher order motion correction schemes.

Affine correction improves on previously described motion correction techniques with the introduction of shear, which allows all linear 3D global transformations to be modeled. Our formulation creates a unified scheme for correction of motion or deformation of any combination of the four building blocks of the affine transformation: translation, rotation, scaling, and shear.

The results presented in Figure 2.4 (columns III-V) were generated using all twenty temporal samplings of the deforming phantom, which corresponds to a 20 fold reduction in imaging time when compared to a gated acquisition. However, in practice, the reduction in imaging time offered by affine motion correction will depend on several factors. Most importantly, this will depend on how well an affine transformation models the deformation of an organ. For example, if the motion of the liver during respiration is well modeled by an affine deformation during 40% of the respiratory cycle, then the scan efficiency will immediately be limited to 40% of a continuous ungated acquisition. Nonetheless, this may still be a significant improvement in scan efficiency when compared to a gated acquisition with no motion compensation, or an acquisition with only translational, or rigid body, motion correction.

As with other correction methods, we have to assume that the entire imaging

volume or slice deforms by one affine transformation. Typically, this assumption will not be valid. A target organ or structure in the field of view may move under the affine motion model, while the other structures remain stationary, or move in a different manner. To reduce image artifacts arising from erroneous motion correction of these surrounding structures, their signal must be suppressed, relative to the desired target object. Contrast agents could be used to enhance the target organ, or alternatively, spatially selective saturation pulses could be used to reduce the signal of the surrounding environment. Receiver coils with highly local sensitivity, such as intravascular coils, could also be used to eliminate signal from surrounding structures.

Motion correction can be implemented either prospectively or retrospectively. In the prospective case, a rectilinear  $k$ -space acquisition would be prescribed for a 3D volume or 2D slice. Before acquiring each line of  $k$ -space, an estimate of the deformation must be made. Equations (2.5) and (2.7) would be used to immediately change the gradient waveforms in order to traverse a modified  $k$ -space trajectory in the Fourier space of the deformed imaging volume. This data would then be stored along the initial trajectory, maintaining a regular and uniform sampling density in  $k$ -space. The difficulty in implementing a prospective motion correction algorithm lies in the computational complexity of extracting the instantaneous 3D affine transformation parameters, and creating gradient waveforms for the modified  $k$ -space trajectory in near real-time. Assuming that noise is spatially uncorrelated, prospective affine motion correction should not affect the noise characteristics of the acquisition, and the SNR should be unaffected.

Affine motion correction is most easily implemented for 3D volumetric imaging, where a stationary imaging volume can be prescribed to contain the desired anatomy during all its motion states. The volumetric excitation would not be changed, and Equations (2.5) and (2.7) could be directly used to modify the two phase encoding gradients and the readout gradient to traverse a new Fourier space trajectory.

For smaller volume excitations, and 2D imaging, it is important to excite the same region of the deforming object during all phases of the motion. The literature has presented slice tracking for rotation, translation, and dilation transformations with a motion component along the slice selection direction. The decomposition of

the 3D affine transformation we have chosen (Equation 2.3) uses an upper triangular shear matrix. This formulation maintains that shearing does not change the object along the  $z$  dimension, which is the slice selection direction in the logical coordinate system commonly used for prescribing MR acquisitions. The upper triangular matrix becomes a lower triangular matrix in Fourier space (Equation 2.5), which means that the signal readout gradient, along the logical  $x$  axis, would not have to be modified. Instead, shear would only affect the phase encoding gradients in the two orthogonal axes. Correction for other shear modes is still possible, because it is always possible to decompose them into rotational and scaling components and an upper triangular shear matrix, as was done in Equation (2.3).

Unlike prospective correction, a retrospective correction technique could be implemented without changing the image acquisition procedure. With each  $k$ -space line that is acquired, a measure of the deformation at that instant would also be stored. After all of the data has been acquired, each  $k$ -space line would be moved to a new position in the Fourier volume, according to Eqs. (2.5) and (2.7), using the transformation parameters associated with that  $k$ -space line.

There are several potential difficulties with the use of a retrospective motion correction approach. With thin 3D slab and 2D slice acquisitions, any through plane motion would violate the requirement for exciting the same regions of the object during all phases of the motion. Prospectively, the slice selection gradients could be modified, but this is not possible to do retrospectively. Also, the transformed lines of  $k$ -space data will likely not lie on a rectilinear grid, and a regridding algorithm will have to be used to regularize the  $k$ -space data before reconstructing the image. The noise characteristics of the corrected data would depend on the interpolation algorithm used for regridding, potentially degrading the image SNR. Finally, the standard spin-warp imaging techniques sample  $k$ -space with a uniform density. After motion correcting, the  $k$ -space lines change to new positions in Fourier space. This can change the regional sampling density, generating frequency areas which are oversampled, and others that are undersampled. The acquisition might have to be repeated a number of times to ensure a minimum sampling density over all of Fourier space. However, changes in sampling density will be small if the physiologic deformations

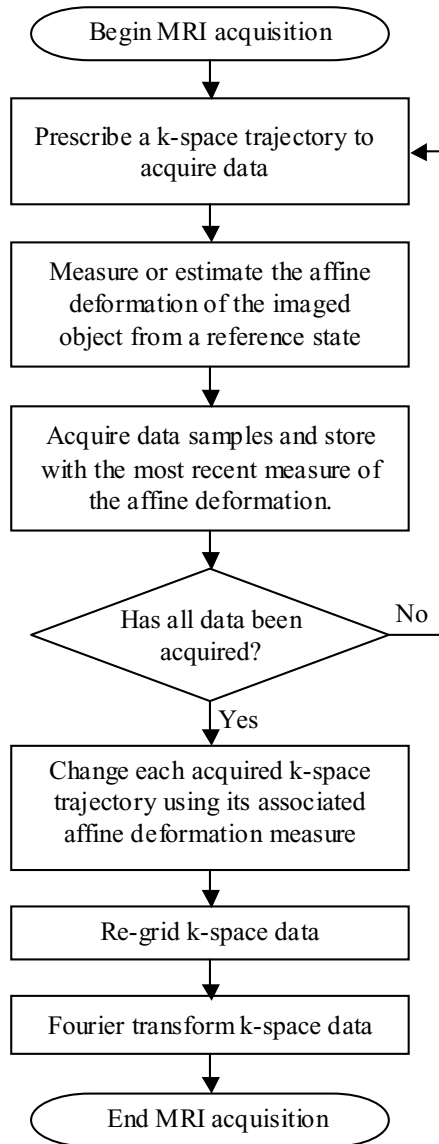


Figure 2.5: Flow diagram for retrospective 3D affine motion correction.

are also small. The magnitude of the displacement of  $k$ -space data is on the same order as the spatial displacement of points in the object.

## 2.4 Conclusion

A method for MR motion correction of objects undergoing a periodic 3D affine deformation has been presented. Results of a computer simulation which validate the proposed 3D affine motion correction strategy have been presented. While the method has been described using a Fourier transform imaging technique, this motion correction method can be directly applied to arbitrary imaging trajectories, such as spiral or radial sampling. Ultimately, the success of any motion correction technique depends on the existence of an accurate model of the motion, and/or the ability to estimate its state at any given time. Innovative MR navigator methods for measuring deformation parameters *in vivo* will be needed.